Half-metallic superconducting triplet spin multivalves

Mohammad Alidoust and Klaus Halterman

Phys. Rev. B **97**, 064517 — Published 26 February 2018

DOI: 10.1103/PhysRevB.97.064517

Half-Metallic Superconducting Triplet Spin MultiValves

Mohammad Alidoust[1] and Klaus Halterman[2]

[1]*Department of Physics, K.N. Toosi University of Technology, Tehran 15875-4416, Iran*
[2]*Michelson Lab, Physics Division, Naval Air Warfare Center, China Lake, California 93555, USA*

(Dated: February 6, 2018)

We study superconductivity spin switching effects in finite-size multivalve structures. We examine $F_1F_2SF_3$ and $F_1F_2SF_3F_4$ hybrids where a singlet superconductor (S) layer is sandwiched among ferromagnet (F) layers with differing thicknesses and magnetization orientations. Our results reveal a considerable number of experimentally viable spin valve configurations that lead to on-off switching of the superconducting phase. For S widths on the order of the superconducting coherence length ξ_0, non-collinear magnetization orientations in adjacent F layers with multiple spin-axes leads to a rich variety of triplet spin-valve effects. Motivated by recent experiments, we focus on samples where magnetization strengths in the F_1 and F_4 layers exist in a fully spin-polarized half metallic phase, and calculate the superconducting transition temperature, spatially and energy resolved density of states, and the spin-singlet and spin-triplet superconducting correlations. Our findings demonstrate that superconductivity in these devices can be completely switched off over a wide range of magnetization misalignment angles due to the generation of equal-spin and opposite-spin triplet pairings.

PACS numbers: 74.78.Na, 74.20.-z, 74.25.Ha

I. INTRODUCTION

Over the last two decades, the interplay of superconductivity and ferromagnetism has fueled interest in exploring ferromagnet (F) and superconductor (S) hybrid structures for low temperature spintronic applications[1–7]. One intriguing consequence of this interplay is the creation of spin-triplet Cooper pairs that was predicted theoretically[5–7]. To confirm the generation of these unconventional pairings, much progress has been made so far, both theoretically and experimentally[8–29]. One of the first signatures of the existence of spin-polarized superconducting correlations was observed in a planar half-metallic Josephson junction[30]. Since a half-metal supports only one spin direction, it was concluded that the supercurrent should be carried by an equal-spin triplet channel.

The two kinds of basic spin valves that have been mainly studied both experimentally and theoretically are F_1SF_2 and SF_1F_2 based structures[5,31–46]. These systems offer simple and controllable platforms that can reveal signatures of spin triplet superconducting correlations. If differing ferromagnetic materials, constituting the left and right F layers are chosen properly, they respond to an external magnetic field in different ways, providing active control of the magnetization misalignment angles through variations in the intensity and direction of an external magnetic field. It was shown that the superconducting transition temperature[47–51] and density of states[13,52–55] reveal prominent signatures of the long-ranged spin-triplet superconductivity[5] as a function of magnetization misalignment. Nevertheless, a direct and clear observation of the equal-spin triplet pairings in superconducting hybrids is still elusive.

In a recent experiment[49] involving a SF_1F_2 spin valve, it was observed that the superconducting critical temperature T_c in MoGe-Ni-Cu-CrO_2, where F_2 is a half-metallic compound, CrO_2, can have a variation as high as $\Delta T_c \sim 800$mK when varying the magnetization misalignment angle. This order of T_c variation is much larger compared to when standard ferromagnets are used [i.e., CuNi-Nb-CuNi[35], CoO_x-Fe1-Cu-Fe1-Pb[40], Co-Cu-Py-Cu-Nb[41], and Co-Nb-Co-Nb[46]], albeit using a relatively strong *out-of-plane* magnetic field of $H \sim 2$T. This was consistent with theory that demonstrated the largest variations in T_c of a SF_1F_2 spin valve[51] occurred when F_2 is a half-metal, rather than a ferromagnet with a smaller exchange energy[48]. A very recent experiment[48], involving the half metal $La_{0.6}Ca_{0.4}MnO_3$, consisted of a LCMO-Au-Py-Cu-Nb stack under the influence of a much weaker *in-plane* magnetic field of $H \sim 3.3$mT to rotate the magnetization orientation. This configuration also demonstrated a slight improvement with $\Delta T_c \sim 150$mK compared to experiments involving standard ferromagnets that yielded $\Delta T_c \sim 50$mK[40], and $\Delta T_c \sim 120$mK[41]. Since strong variations in T_c can be representative of singlet superconductivity weakening and its conversion to the triplet channel, it is of fundamental interest to create spin valve structures with the largest variations in T_c by a *weak* external magnetic field. On the one hand, it can provide unambiguous signatures of the presence of equal-spin triplet correlations under magnetization rotation. On the other hand, by restricting the magnetization variations to reside in-plane, the overall magnetization state in the ferromagnet can be manipulated with much weaker fields. This low-field magnetization control considerably increases device reliability and provides an effective spin switch for technological purposes.

In this paper, we introduce the $F_1F_2SF_3$ and $F_1F_2SF_3F_4$ multivalves (depicted in Fig. 1), where the two outer F layers are half-metallic. The presence of the additional ferromagnetic layers amplifies the singlet-triplet conversion process, leading to a larger spin valve effect compared to standard spin valves described above. We show this by considering a wide range of layer thicknesses and magnetizations to achieve a broad critical temperature variation as the magnetization in one of the F layers rotates. As mentioned earlier, the transition temperature of a spin valve system[47–49,51] and the density of states[52–55] are two experimental quantities that can determine the degree in which triplet pair conversion takes place for a given device.

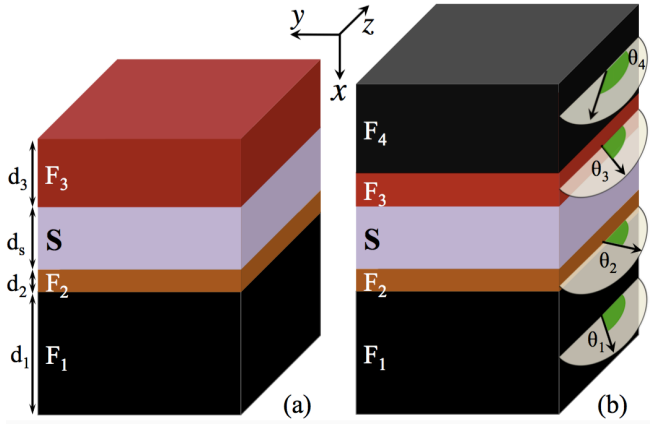

FIG. 1. Schematic of the superconducting triplet spin multivalves: (a) $F_1F_2SF_3$ and (b) $F_1F_2SF_3F_4$ structures. The interfaces reside in the yz plane and the thickness of a layer i=1-4 is marked by d_i. The magnetization of the F layers is shown by an arrow that can make arbitrary angles with respect to the z axis marked by θ_i.

Our investigation is within the ballistic regime using a microscopic self-consistent formalism that can accommodate the large variation in energy scales present in the problem. In particular, the multivalve structures considered here contain conventional ferromagnets with relatively weak exchange fields ($h/E_F \ll 1$) in addition to the surrounding half metals ($h/E_F = 1$). Our results demonstrate that, stemming from nontrivial interlayer spin-valve effects, superconductivity can be effectively switched on or off over a wide range of relative magnetization misalignment angles. We note that this feature is absent or occurs to a limited extent in the previously studied[51,56] individual F_1SF_2 and SF_1F_2 spin-valves. We complement the T_c studies by investigating various pair correlations and the corresponding local density of states, where the emergence of a zero-energy peak is associated with the presence of equal-spin triplet correlations.

The rest of the paper is organized as follows. We first present an overview of the theoretical framework used. In Sec. II A we study the superconducting transition temperature for two multivalve configurations. In the fourth subsection II B we present the corresponding local density of states, paying particular attention to the DOS at zero energy. Lastly, we present the singlet and triplet superconducting correlations generated and discuss their behavior in Sec. II C. Finally, we give concluding remarks in Sec. III.

II. THEORY AND RESULTS

To accurately describe the ballistic multivalve configurations displayed in Fig. 1, we solve the spin-dependent Bogoliubov-de Gennes (BdG) equations in a fully self-consistent[57] manner. In this formalism we denote the quasiparticles' energy and their associated probability amplitudes by ϵ_n, $u_{n\sigma}$, and $v_{n\sigma}$ ($\sigma =\uparrow,\downarrow$), respectively:

$$\begin{pmatrix} \mathcal{H}_0 - h_z & -h_x + ih_y & 0 & \Delta(x) \\ -h_x - ih_y & \mathcal{H}_0 + h_z & \Delta(x) & 0 \\ 0 & \Delta^*(x) & -(\mathcal{H}_0 - h_z) & -h_x - ih_y \\ \Delta^*(x) & 0 & -h_x + ih_y & -(\mathcal{H}_0 + h_z) \end{pmatrix} \times \begin{pmatrix} u_{n\uparrow} \\ u_{n\downarrow} \\ v_{n\uparrow} \\ v_{n\downarrow} \end{pmatrix} = \epsilon_n \begin{pmatrix} u_{n\uparrow} \\ u_{n\downarrow} \\ v_{n\uparrow} \\ v_{n\downarrow} \end{pmatrix}, \quad (1)$$

in which $\Delta(x)$ represents the pair potential, calculated self-consistently as shown below [Eq. (3)]. For the in-plane magnetization rotations considered here, the components of the exchange field $\boldsymbol{h}$ in each of the F layers take the form: $\boldsymbol{h} = (h_x(x), h_y(x), h_z(x))$, so that the exchange field which vanishes in the S layer, can in general vary between the ferromagnet layers. The free-particle Hamiltonian $\mathcal{H}_0(x)$ is defined as,

$$\mathcal{H}_0(x) \equiv \frac{1}{2m}\left(-\frac{d^2}{dx^2} + k_y^2 + k_z^2\right) - E_F + U(x), \quad (2)$$

where E_F denotes the Fermi energy, and $U(x)$ is a spin-independent scattering potential. The multivalve layers in Fig. 1, are translationally invariant in the yz plane and hence quasiparticle motion in this plane is appropriately described by the good quantum numbers k_y and k_z. For this reason, all spatial variations take place in the x direction, and the system is considered quasi-one dimensional.

Ferromagnetism and superconductivity are two competing types of ordering and their simultaneous existence in space results in nontrivial spatial profiles for the pair potential $\Delta(x)$. Therefore, to account properly for proximity effects, it is necessary to obtain the pair potential in a self-consistent manner via:

$$\Delta(x) = \frac{g(x)}{2}\sum_n^{\omega_D}[u_{n\uparrow}(x)v^*_{n\downarrow}(x) + u_{n\downarrow}(x)v^*_{n\uparrow}(x)]\tanh\left(\frac{\epsilon_n}{2T}\right), \quad (3)$$

where $g(x)$ is the pair coupling constant that is nonzero solely inside the superconductor layer and the sum above is restricted to the quantum states with positive energies below the Debye energy cutoff ω_D.

To compute the transition temperature, we use the fact that $\Delta(x)/\Delta_0 \ll 1$ close to the critical temperature, where Δ_0 is the bulk pair potential at zero temperature, $T = 0$. In this regime, the self-consistency equation [Eq. (3)] can be linearized near the transition through a perturbative expansion of the quasiparticle amplitudes and energies and retaining terms to first order. As part of the linearization process, the pair potential $\Delta(x)$ and quasiparticle amplitudes are Fourier expanded in a sine-wave basis. For example, the zeroth-order wavefunctions are written, $u^0_{n\sigma} = \sqrt{2/d}\sum_p u^\sigma_{np}\sin(k_p x)$ and $v^0_{n\sigma} = \sqrt{2/d}\sum_p v^\sigma_{np}\sin(k_p x)$. Using standard perturbation theory techniques described elsewhere,[35,58] we arrive at the following matrix eigenvalue problem:

$$\Delta_i = \sum_q J_{iq}\Delta_q, \quad (4)$$

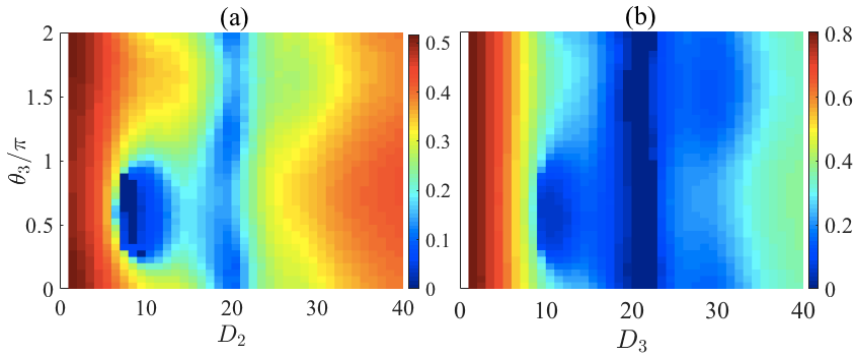

FIG. 2. The normalized transition temperature as a function of magnetization rotation in F_3 layer of a $F_1F_2SF_3$ spin multivalve. In panel (a) the thickness of F_2 layer changes while in (b) the thickness of F_3 varies.

where the Δ_q are the first-order expansion coefficients for $\Delta(x)$, and J_{iq} are the matrix elements written entirely in terms of zeroth-order quantities:

$$J_{iq} = \frac{gN_0}{8\pi k_F d}\int d\epsilon_\perp \sum_n \sum_m \left\{ \frac{\mathcal{F}_{qnm}\mathcal{F}_{inm}}{\epsilon_n^u - \epsilon_m^v}\tanh\left(\frac{\epsilon_n^u}{2T}\right) + \frac{\mathcal{F}_{qmn}\mathcal{F}_{imn}}{\epsilon_n^v - \epsilon_m^u}\tanh\left(\frac{\epsilon_n^v}{2T}\right)\right\}, \quad (5)$$

where $\varepsilon_\perp = 1/(2m)(k_y^2 + k_z^2)$ is the quasiparticle kinetic energy in the transverse direction, N_0 is the density of states at the Fermi energy, and $\varepsilon_n^{u,v}$ are the unperturbed zeroth-order energies. The zeroth-order quasiparticle amplitudes $(u_{n\sigma}^0,\ v_{n\sigma}^0)$ and corresponding energies $(\varepsilon_n^u,\varepsilon_n^v)$ are found by solving Eq. (1) with $\Delta(x) = 0$. We also define, $\mathcal{F}_{qnm} = \pi\sqrt{2d}\sum_{p,r} K_{qpr}(u_{mp}^{\uparrow}v_{nr}^{\downarrow} + u_{mp}^{\downarrow}v_{nr}^{\uparrow})$, where

$$gK_{qpr} = (2/d)^{3/2}\int_0^d dx g(x)\sin(k_q x)\sin(k_p x)\sin(k_r x). \quad (6)$$

Experimentally accessible information regarding the quasiparticle spectra is contained in the local density of single-particle excitations in the system. This includes zero-energy signatures in the form of peaks[52–55] in the density of states (DOS), which can reveal the emergence of equal-spin triplet pairings in either the ferromagnet[53] or superconductor[51] regions. The total local density of states, $N(x,\epsilon)$, includes contributions from both the spin-up and spin-down quasiparticle states: $N(x,\epsilon) = N_\uparrow(x,\epsilon) + N_\downarrow(x,\epsilon)$, where,

$$N_\sigma(x,\epsilon) = -\sum_n \Big\{|u_{n\sigma}(x)|^2 f'(\epsilon-\epsilon_n) + |v_{n\sigma}(x)|^2 f'(\epsilon+\epsilon_n)\Big\}, \quad (7)$$

in which $f'(\epsilon) = \partial f/\partial\epsilon$ is the derivative of the Fermi function.

In order to study the various superconducting correlations that can arise, we define[8,59] the triplet pair amplitudes in terms of the field operators:

$$f_0(x,t) = \frac{1}{2}\left[\langle\psi_\uparrow(x,t)\psi_\downarrow(x,0)\rangle + \langle\psi_\downarrow(x,t)\psi_\uparrow(x,0)\rangle\right], \quad (8a)$$

$$f_1(x,t) = \frac{1}{2}\left[\langle\psi_\uparrow(x,t)\psi_\uparrow(x,0)\rangle - \langle\psi_\downarrow(x,t)\psi_\downarrow(x,0)\rangle\right], \quad (8b)$$

$$f_2(x,t) = \frac{1}{2}\left[\langle\psi_\uparrow(x,t)\psi_\uparrow(x,0)\rangle + \langle\psi_\downarrow(x,t)\psi_\downarrow(x,0)\rangle\right]. \quad (8c)$$

where t is the relative time in the Heisenberg picture. If we consider the quantization axis fixed along the z axis, the triplet amplitudes $(f_0(x,t),f_1(x,t),f_2(x,t))$ can be written in terms of the quasiparticle amplitudes:[8,59]

$$f_0(x,t) = \frac{1}{2}\sum_n \left[u_{n\uparrow}(x)v_{n\downarrow}^*(x) - u_{n\downarrow}(x)v_{n\uparrow}^*(x)\right]\zeta_n(t), \quad (9a)$$

$$f_1(x,t) = -\frac{1}{2}\sum_n \left[u_{n\uparrow}(x)v_{n\uparrow}^*(x) + u_{n\downarrow}(x)v_{n\downarrow}^*(x)\right]\zeta_n(t), \quad (9b)$$

$$f_2(x,t) = -\frac{1}{2}\sum_n \left[u_{n\uparrow}(x)v_{n\uparrow}^*(x) - u_{n\downarrow}(x)v_{n\downarrow}^*(x)\right]\zeta_n(t), \quad (9c)$$

where $\zeta_n(t)$ is given by,

$$\zeta_n(t) = \cos(\epsilon_n t) - i\sin(\epsilon_n t)\tanh\left(\frac{\epsilon_n}{2T}\right). \quad (10)$$

We consider an in-plane[48] Stoner-type exchange field for each magnetic layer,

$$\boldsymbol{h}_i = h(0,\sin\theta_i,\cos\theta_i), \quad (11)$$

where h_i are the magnitudes of the exchange field in each layer denoted by i, and θ_i are the angles that $\boldsymbol{h}_i$ make with the z-axis (see Fig. 1). In situations where it is more convenient to align the quantization axis with the local exchange field direction, we perform a spin rotation using the transformations found in the Appendix. The result is

$$f_0' = f_0\cos\theta_i + i\sin\theta_i f_2, \quad (12)$$

$$f_1' = f_1, \quad (13)$$

$$f_2' = \cos\theta_i f_2 + i\sin\theta_i f_0. \quad (14)$$

When presenting results, we normalize all lengths by the Fermi wavevector k_F, e.g., $D_i = k_F d_i$, $X = k_F x$. We set the superconducting coherence length to the normalized value of $k_F\xi_0 = 100$. The half-metallic layers have fixed width $D_{1,4} = 100$ The quasiparticle energies are scaled by the bulk superconducting gap Δ_0, and the critical temperature of a sample by T_0, the transition temperature of its bulk counterpart. The local DOS is normalized by the DOS of a normal metal.

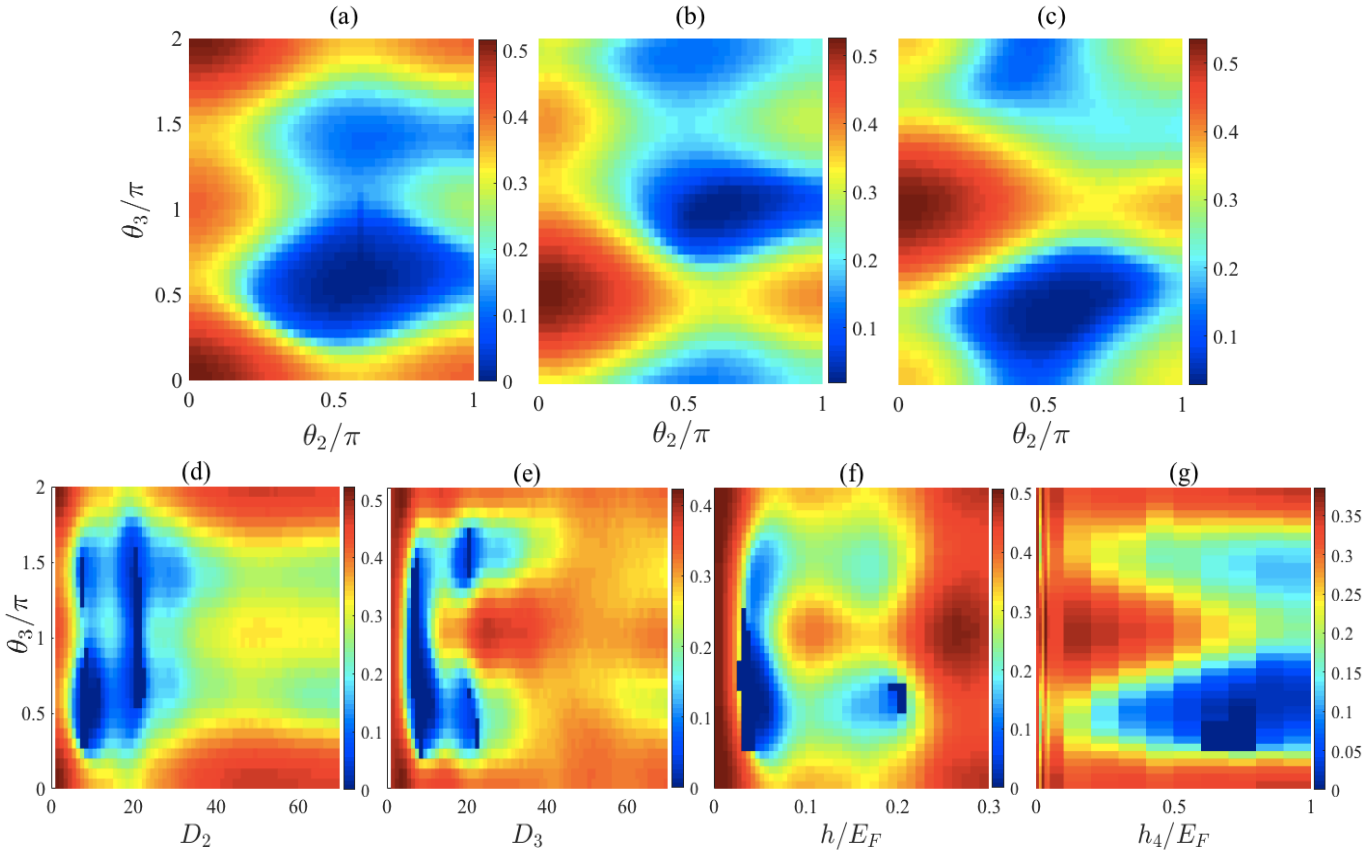

FIG. 3. The normalized transition temperature T_c/T_0 of a $F_1F_2SF_3F_4$ structure where the outer magnetic layers are in a half-metallic phase in panels (a)-(e). In panels (a)-(c) the critical temperature is plotted as a function of θ_2 and θ_3, the magnetization orientation in F_2 and F_3 layers. Here in (a), (b), and (c), we rotate the magnetization of F_4 so that $\theta_4 = 0, 0.5\pi$, and π, respectively. In panels (d) and (e), the critical temperature is plotted as a function of magnetization rotation in the F_3 layer and thicknesses of F_2 and F_3 layers: $D_{2,3}$. Panel (f) shows T_c/T_0 vs θ_3 and magnetization strength in both F_2 and F_3. Here, we assume identical magnitudes to the exchange fields, i.e., $h_2 = h_3 = h$. In (g), we plot T_c/T_0 vs the magnetization strength of F_4 and θ_3 while $h_1 = E_F$, supporting only one spin direction.

A. Transition Temperature

In this section, we present results for the transition temperature T_c by solving the matrix eigenvalue equation in Eq. (4). The procedure for identifying T_c involves varying the temperature T and calculating the eigenvalues[35,58]. At the transition temperature, the largest eigenvalue is unity, while if $T > T_c$ all eigenvalues are less than unity. In Fig. 2, the normalized transition temperature T_c/T_{c0} of the $F_1F_2SF_3$ multivalve configuration is shown (see Fig. 1(a)), where F_1 is a half-metal (with $h_1 = E_F$). For both panels we have set $D_1 = 100$, $D_S = 250$, $\theta_1 = 0, \theta_2 = \pi/2$, and $h_2 = h_3 = 0.05E_F$. In Fig. 2(a) we set $D_3 = 10$ and plot T_c vs θ_3 and D_2. In Fig. 2(b) the thickness of the F_2 is fixed at $D_2 = 10$ and T_c is plotted vs θ_3 and D_3. As seen, the critical temperature approaches zero in the window $0.35\pi \lesssim \theta_3 \lesssim 0.8\pi$ and $D_2 \sim 10$. The critical temperature shows a nonmonotonic behavior vs both θ_3 and D_2 with two minima at $D_2 \sim 10$ and $D_2 \sim 20$. Similar trends are obtained when D_3 varies. Nonetheless, Fig. 2(b) shows an effectively stronger spin valve effect with T_c spanning the range $0 < T_c/T_0 < 0.8$, compared to Fig. 2(a) which has $0 < T_c/T_0 < 0.5$. In addition, at $D_3 \sim 20$, the critical temperature is vanishingly small for all values of θ_3. These results demonstrate an effective spin switch that can turn superconductivity on or off using a multivalve $F_1F_2SF_3$ configuration with experimentally accessible parameters.

Next, we incorporate an additional half-metallic layer, and consider the superconducting critical temperature of the $F_1F_2SF_3F_4$ multivalve in Fig. 3. Having the outer F_1 and F_4 layers half-metallic with $h_{1,4} = E_F$ (and thus only one spin band at the Fermi level) maximizes the generation of equal-spin triplet pairs. In Figs. 3(a), 3(b), and 3(c) the normalized critical temperature T_c/T_0 is plotted as a function of the magnetization orientation angles in the $F_{2,3}$ layers θ_2 and θ_3. Here, the weaker inner ferromagnets have the exchange fields $h_2 = h_3 = 0.05E_F$ and widths $D_2 = D_3 = 10$. The superconductor has $D_S = 250$, corresponding to a relative thickness $d_s/\xi_0 = 2.5$. In Figs. 3(a), 3(b), and 3(c) the magnetization in the right half-metal F_4 is set along z, y, and -z, respectively, while the orientation of the left half-metal F_1 is fixed along the z direction. As seen, in Fig. 3(a), the critical temperature is zero at $\theta_{2,3} \sim \pi/2$. Thus, at this magnetization configuration, the system transitions to a normal resistive state for *all* temperatures. By changing the magnetization align-

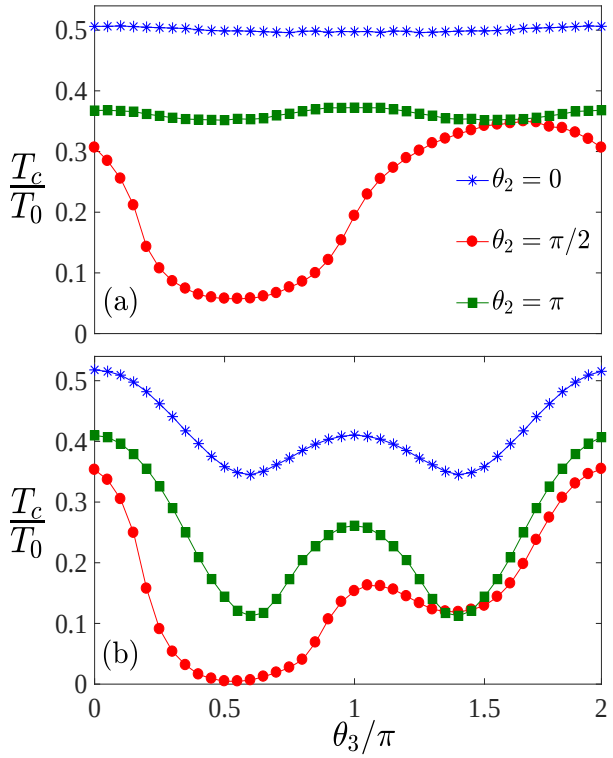

FIG. 4. The normalized transition temperature as a function of θ_3, the magnetization rotation angle in F_3. Three different magnetization orientations in the F_2 region are considered: $\theta_2 = 0, \pi/2$, and π. Panel (a) illustrates the variation in the critical temperature of the $F_1F_2SF_3$ structure, while (b) corresponds to a $F_1F_2SF_3F_4$ configuration.

ment in F_4, panels (b) and (c) demonstrate that regions of very low T_c (blue regions) shift to larger θ_2 and θ_3. The critical temperature mappings in (a)-(c) suggest that a large number of combinations of magnetization alignments leads to effective spin switches with large critical temperature variations $\Delta T_c(\theta_i) = T_{c,\max}(\theta_i) - T_{c,\min}(\theta_i)$. In Fig. 3(b), as seen, the minimum of T_c exceeds zero and also regions of very small T_c occur over narrower angular ranges of θ_2 and θ_3.

Next in Fig. 3 we investigate how the critical temperature is modified when varying θ_3 (we set $\theta_2 = \pi/2$) and (d) the dimensionless thickness D_2 ($D_3 = 10$) or (e) the thickness D_3 ($D_2 = 10$). For certain ferromagnet widths $D_{2,3} \sim 10$ and 20, the critical temperature is severely diminished for a broad range of θ_3. Indeed, Fig. 3(d) shows that if the system is in a superconducting state at $T = 0$, superconductivity is completely switched off for orientations with $\theta_3 \sim \pi/2$ and $\sim 1.5\pi$. This type of switching effect occurs over an extended angular range $0.5\pi \lesssim \theta_3 \lesssim 1.5\pi$ for $D_3 \sim 20$, indicative of a strong spin valve effect in this regime. The same feature appears in Fig. 3(e) except now the on-off superconductivity switching regime occurs at $D_3 = 10$ and broadens to $0.2\pi \lesssim \theta_3 \lesssim 1.5\pi$.

The choice of relatively weak ferromagnets for F_2 and F_3 generates opposite-spin triplet correlations in those regions and a subsequent conversion into spin-triplet pairs that can propagate within the half-metallic regions, modifying T_c. To identify the optimal ferromagnetic strengths, we show in Fig. 3(f) the critical temperature vs the normalized magnetization strength in both F_2 and F_3. For simplicity, we set $h_2 = h_3 = h$. It is evident that there is a broad region spanned by h and θ_3 in which $T_c \approx 0$, creating an effective superconductivity on-off switch. In particular, superconductivity is shown to disappear at any temperature when $0.2\pi \lesssim \theta_3 \lesssim \pi$ and $0.03 \lesssim h/E_F \lesssim 0.06$. Nonetheless, $\theta_3 = 0.5\pi$ and 1.5π, overall, provides smaller critical temperatures within $0.03 \lesssim h/E_F \lesssim 0.22$. These results demonstrate that the use of ferromagnets $F_{2,3}$ with $h/E_F \ll 1$ causes the greatest decline in the superconducting state. Below, this will be discussed in terms of the population of both the equal-spin and opposite-spin triplet correlations in each relevant region of the spin valve. Lastly, in a similar fashion we show the importance of using half-metallic outer layers to achieve enhanced spin valve effects. In Fig. 3(g), we exhibit the critical temperature vs the normalized exchange energy h_4/E_F. The ferromagnets again have $D_{2,3} = 10$ and $h_{2,3}/E_F = 0.05$. The magnetization in F_2 is aligned according to $\theta_2 = 0.5\pi$ (along the y-direction) and the first outer layer has $h_1 = E_F$. The exchange field strength in h_4 varies from 0 to E_F, or equivalently, from a nonmagnetic normal metal to a fully spin polarized half-metal. Consistent with previous studies[48,49,51], the results shown here demonstrate that when the layer adjacent to the weak ferromagnet has one spin state present at the Fermi energy, the greatest variations in T_c as a function of magnetization rotation can occur. Switching between superconducting and normal resistive states has previously been found in F_1SF_2[56] and SF_1F_2 [51] structures. By incorporating multiple half-metallic layers, the variations in T_c found here, with a fairly thick S layer, are considerably larger than what has been previously reported for the simpler SF_1F_2 and F_1SF_2 counterparts.

The conversion of opposite-spin triplet pairs into equal-spin triplet pairs is enhanced by coupling a weaker ferromagnet with the half-metal due in part to the preservation of phase coherence that would otherwise be destroyed by the single-spin half-metal. To exemplify this, and to compare the relative strengths of the two types of spin valves, we present in Fig. 4, the normalized T_c as a function of magnetization orientation θ_3 for both the (a) $F_1F_2SF_3$ and (b) $F_1F_2SF_3F_4$ types of structures. The thickness of the superconducting layer is fixed at $D_S = 250$, which serves to effectively illustrate which device configuration leads to the largest ΔT_c variations. The ferromagnetic layers F_1 and F_4 are half metallic, while the other layers are much weaker, standard ferromagnets. The remaining parameters are set identical to the cases previously shown. We examine three magnetization orientations in the F_2 layer: $\theta_2 = 0, \pi/2, \pi$, while rotating θ_3 continuously from 0 to 2π. In the top panel, the angle $\theta_2 = 0$ corresponds to a FSF configuration, while for the lower panel it coincides with a $F_1SF_2F_3$ structure. Thus, by appropriately varying the magnetizations, the multivalves can be reduced to their simpler F_1F_2S and F_1SF_2 spin-valve counterparts. As seen, $\theta_2 = 0$ induces the weakest variations in T_c for both devices. The case with $\theta_2 = \pi$ introduces moderate variations in T_c, while the largest changes arise when $\theta_2 = \pi/2$, corresponding to the spin multivalve configurations introduced in this paper. It is evident that

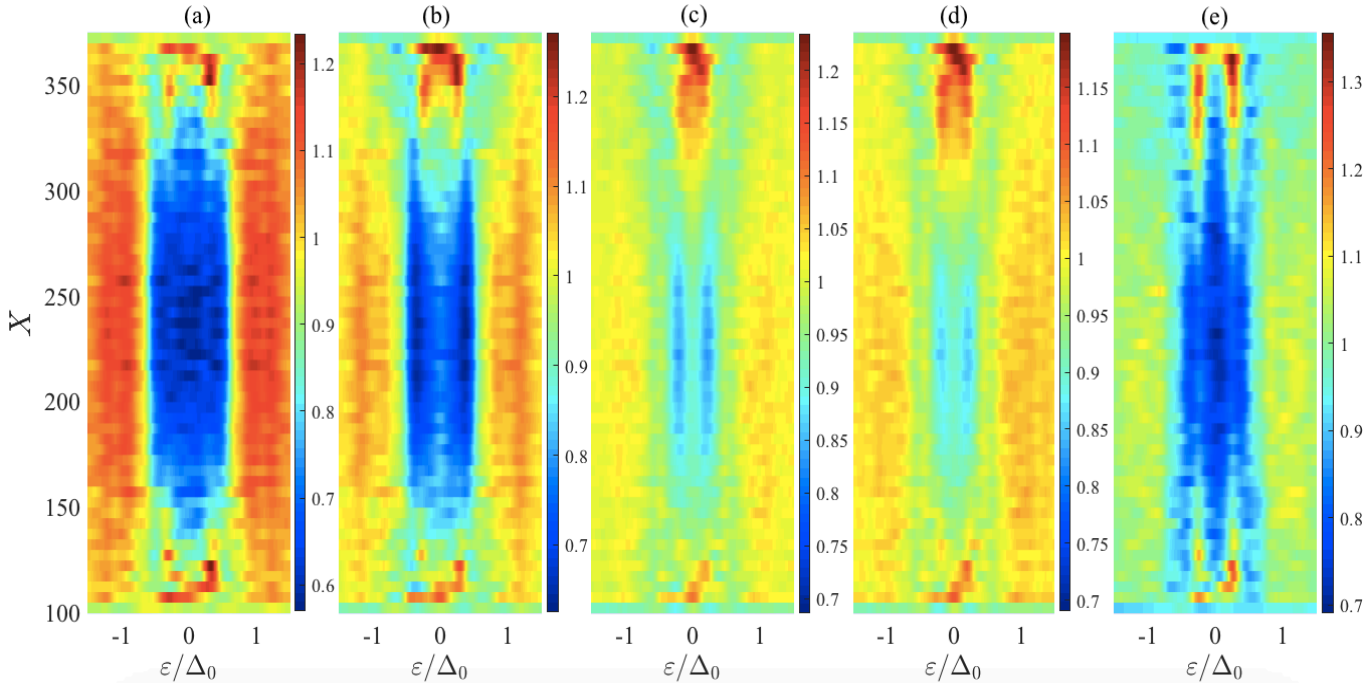

FIG. 5. The normalized spatial ($X \equiv k_F x$) and energy (ε/Δ_0) resolved density of states of a ballistic $F_1F_2SF_3F_4$ structure. The $F_{1,4}$ layers are in the half-metallic phase, and the magnetization in the $F_{1,2,4}$ layers is fixed along the z axis. Each panel (a)-(e) corresponds to a different magnetization orientation, with $\theta_3 = 0, \pi/3.6, \pi/2, \pi/1.65$, and π, respectively.

the critical temperature for the $F_1F_2SF_3F_4$ multivalve reaches zero when $\theta_2 = \pi/2$ and $0.48\pi \lesssim \theta_3 \lesssim 0.52\pi$, which is equivalent to a normal resistive state. Thus, it is apparent that the $F_1F_2SF_3F_4$ device can provide stronger variations in the superconducting critical temperature compared to $F_1F_2SF_3$ and simpler spin valves.

B. Density of States

The study of single-particle excitations in these systems can reveal important signatures in the proximity induced singlet and triplet pair correlations. A useful experimental tool that probes these single-particle states is tunneling spectroscopy, in which the local DOS, $N(x, \varepsilon)$, can be measured as a function of position x and energy ε. In Fig. 5, the local DOS is shown as a function of the normalized quasiparticle energy ϵ/Δ_0 and normalized location X within the F_2SF_3 region of a $F_1F_2SF_3F_4$ multivalve. All plots are normalized to the corresponding DOS in a bulk sample of S material in its normal state. To be consistent, we use the same layer thicknesses and exchange field magnitudes found in Fig. 3(a). In Figs. 5(a)-5(e) the magnetization in the F_3 layer is rotated incrementally according to $\theta_3 = 0, \pi/3.6, \pi/2, \pi/1.65$, and π. The $F_{1,2,4}$ layers have their magnetizations oriented along z, i.e., $\theta_{1,2,4} = 0$. We note that, as seen in Fig. 3, the variation of both θ_2 and θ_3 results in a fairly wide range of magnetization directions where $T_c \sim 0$, and thus in those cases the system is not superconducting at any temperature. Hence, $\theta_2 = 0$ is chosen so that T_c is nonzero over a wider range in parameter space. In (a), the magnetizations in each layer are collinear and directed along z, allowing only the opposite-pair correlations to exist. Although there is no gap in the energy spectrum, near the center of the superconductor ($X \sim 225$), traces of the BCS-like

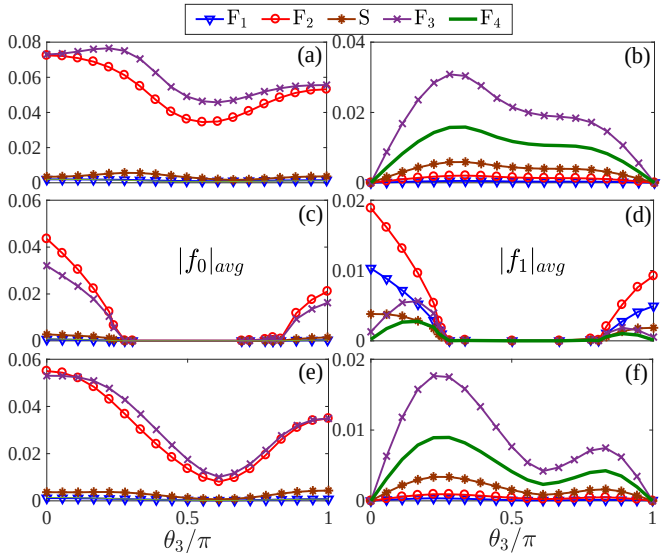

FIG. 6. The opposite-spin (f_0) and equal-spin (f_1) pairings vs θ_3, averaged over each region in a $F_1F_2SF_3F_4$ structure where $F_{1,4}$ are half-metallic. In the top row, (a) and (b), we set $\theta_2 = 0$, in the middle row, (c) and (d), $\theta_2 = \pi/2$, while in the bottom row, (e) and (f), θ_2 is equal to π.

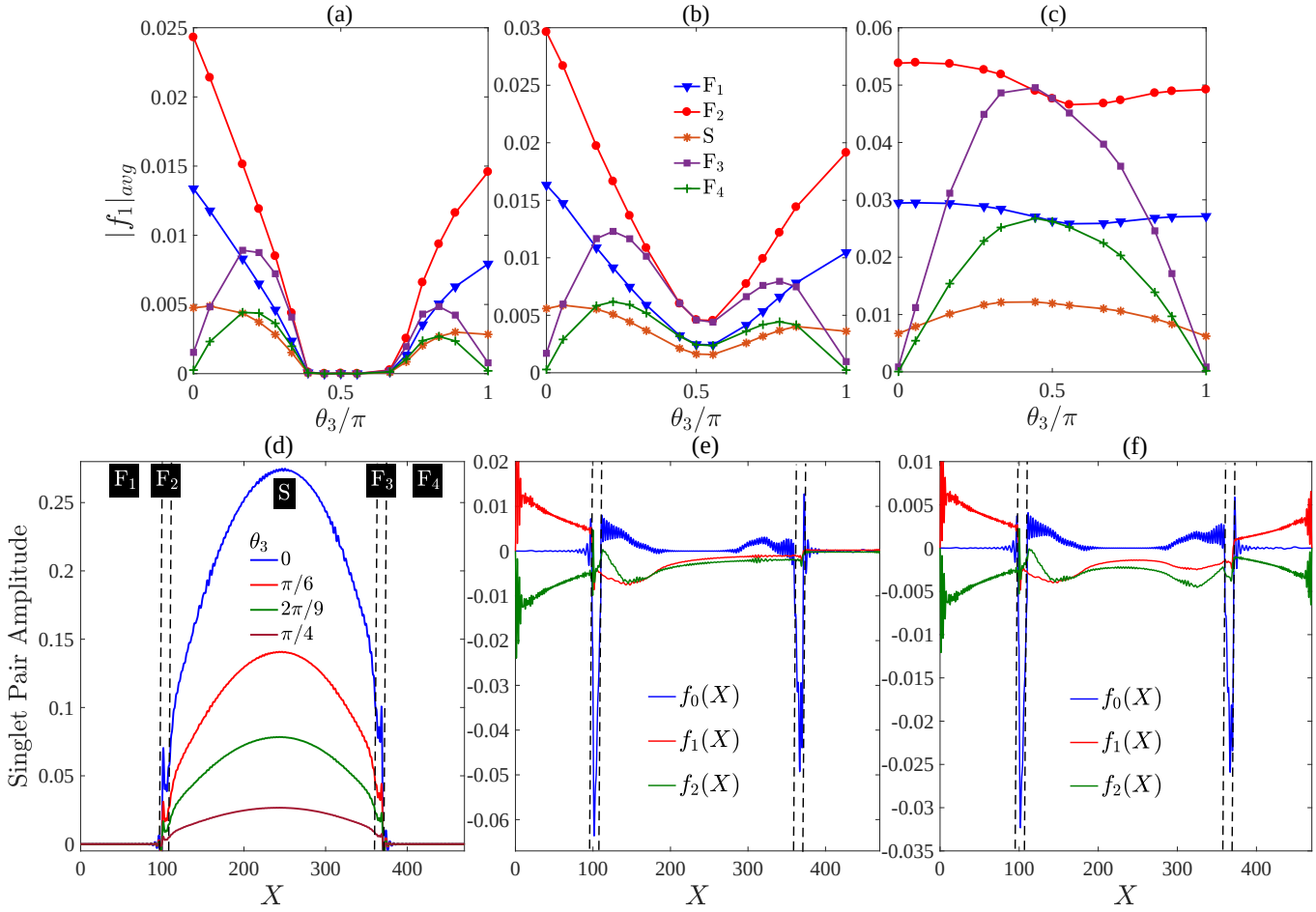

FIG. 7. Top row: Effects of the superconductor width on the behavior of the equal spin triplets f_1 as a function of the magnetization orientation angle θ_3. Three cases are considered: (a) $D_S = 260$, (b) $D_S = 270$, and (c) $D_S = 400$. The legend identifies each region of the $F_1F_2SF_3F_4$ multivalve in which f_1 is averaged over. Bottom row: The singlet (d) and triplet amplitudes ((e) and (f)) shown as a function of dimensionless position throughout the entire $F_1F_2SF_3F_4$ spin valve. Here $D_S = 250$, and $\theta_2 = \pi/2$. The dashed vertical lines identify the interfaces bounding the thin ferromagnets F_2 and F_3 (the regions are labeled in (d)). In (e) the magnetization orientation angle $\theta_3 = 0$, and in (f) $\theta_3 = \pi/6$.

energy structure are seen. The self-consistent proximity effects within the vicinity of the interfaces (found near the endpoints of the X range) however result in an increase of subgap states ($|\varepsilon/\Delta_0| < 1$). We see in Fig. 3(b) that the deviation of the magnetization orientation in F_3 from 0 to $\pi/3.6$ results in a peak at zero energy near the S/F_3 interface ($x \sim 360$), and within the S region. As Fig. 5(c) and 5(d) depict, as the magnetization rotates closer to the $\pi/2$ orientation, this zero energy peak region becomes more localized and pronounced in energy, extending deeper into the S layer. Finally, in Fig. 3(e), the relative magnetizations are again collinear, with the magnetization in F_3 antiparallel to the z-axis ($\theta_3 = \pi$), resulting in the disappearance of the zero energy mode and subsequent splitting into separate Andreev bound states. Note that the microscopic method used here accounts for the significant band curvature near the Fermi energy arising from the strong spin-splitting effects of the half-metallic layers, as evidenced by the particle-hole asymmetry in the DOS.[51,60,61]

C. Superconducting Correlations

To correlate the spin-triplet superconducting correlations to the nonmonotonic behavior of T_c, we plot the opposite-spin (f_0) and equal-spin (f_1) pair correlations in Fig. 6. We have averaged f_0 and f_1 over each region separately, identified by F_1, F_2, S, F_3, and F_4. In this fashion, one can readily evaluate the spatial distribution of the different pairings, denoted by $|f_0|_{avg}$ and $|f_1|_{avg}$. We consider the $F_1F_2SF_3F_4$ configuration with the same parameter values used in Fig. 3(a). In Figs. 6(a) and 6(b) we set $\theta_2 = 0$, in 6(c) and 6(d) $\theta_2 = \pi/2$, and in 6(e) and 6(f) $\theta_2 = \pi$. The outer half-metals also have $\theta_1 = \theta_4 = 0$. For the top and bottom rows when $\theta_2 = 0$, and $\theta_2 = \pi$, respectively, all of the magnetic layers have collinear relative magnetizations (except of course for F_3, which has θ_3 varying). In these configurations, we see that f_1 is zero at $\theta_3 = 0$ and $\theta_3 = \pi$, since then, all layers are collinear with a single quantization axis which prohibits the generation of equal-spin triplet pairs. We see that f_0 exhibits the same behavior as T_c at $\theta_2 = 0, \pi/2, \pi$, i.e., decreases as θ_3 approaches $\sim \pi/2$. The f_1 triplet pair-

ing however increases simultaneously, demonstrating a direct link between the appearance of equal-spin correlations and a decrease in T_c. In cases where $\theta_2 = 0$ and π, we see that the f_1 correlation has a large amplitude in the right half-metal F_4. It is also evident that f_0 is negligible in the half-metallic regions F_1 and F_4, since this opposite spin triplet channel is energetically unstable in the regions with only one spin band present. The magnetization direction in F_2 results in drastic changes: As can be seen in Figs. 6(c) and 6(d), f_1 correlations penetrate all regions throughout the multivalve and both f_0 and f_1 vanish within $0.35\pi \lesssim \theta_3 \lesssim 0.75\pi$ which is consistent with the T_c results where superconductivity disappears in the middle S layer.

The superconductor width plays a key role in the range of magnetization angles that result in strong spin valve effects. In the top row of Fig. 7, three larger S widths corresponding to $D_S = 260, 270$, and $D_S = 400$ are presented. Previously in Fig. 3(a) we found that for $D_S = 250$ and $\theta_2 = \pi/2$, there was a sizable range of angles θ_3 in which the singlet correlations vanished at $T = 0$. In these regions of parameter space, the triplet correlations must also vanish as demonstrated in Fig. 6(c) and (d). If the thickness of superconductor layer increases, the pair breaking effects of the surrounding magnets become less detrimental to superconductivity, and the angular window that results in the system transitioning to a normal resistive metal narrows and eventually disappears altogether. For instance, in Fig. 7(a), although the overall trends are the same, the interval in which $f_1 = 0$ has been reduced to $0.4\pi \lesssim \theta_3 \lesssim 0.65\pi$ compared to the $D_S = 250$ case in Fig. 6(d). For $D_S = 270$ in Fig. 7(b), the triplet correlations f_1 now pervade every region of the spin valve. Instead of vanishing over a certain range of magnetization orientation angles, f_1 dips to a minimum at $\theta_3 \approx \pi/2$ in every layer, including the superconductor. Finally, if the S layer is increased to $D_S = 400$ as shown in (c), the behavior of f_1 changes drastically throughout the system. The three layers consisting of S, F_3 and the half-metal F_4, which previously had dips in f_1 at $\theta_3 \approx \pi/2$, now have their situations reversed so that the f_1 triplet population is enhanced in those regions. Thus for example, for thin S widths the f_1 correlations in the half-metal F_4 are constrained to vanish over a range of magnetization misalignment angles, including at $\theta_3 = \pi/2$, and as the S width increases, the constraint is lifted and what was once an absence or minimum of f_1, now peaks for the magnetically inhomogenous situation $\theta_3 \approx \pi/2$.

Further information can be gathered from the spatial dependence of the pair correlations. In Fig. 7(d), the singlet pair correlations are shown as a function of dimensionless position X for several magnetization orientations θ_3. The parameter values used here are identical to those implemented in Figs. 6(c) and (d), where $D_S = 250$ and $\theta_2 = \pi/2$. Each curve represents a different magnetization orientation described by the angle θ_3 shown in the legend. As observed in Fig. 3, T_c exhibits considerable variations when rotating from $\theta_3 = 0$, where all magnetizations are aligned along the z direction (except in F_2, which is directed along y), to $\theta_3 = \pi/2$, where the magnetizations between the ferromagnets and half-metals are orthogonal. Indeed, the transition temperature rapidly diminishes until eventually the system transitions to the normal state for all temperatures. This is reflected in the self consistent singlet pair correlations at $T = 0$ (Fig. 7(d)), where the rapid decline in the S region as a function of θ_3 is clearly evident. The singlet correlations of course vanish in the half-metallic regions where only one spin state is permitted. Moreover, due to the asymmetric magnetization profile, the singlet profile is not symmetric, exhibiting a greater presence of singlet correlations in F_3 compared to F_2. Due to the singlet-triplet conversion that takes place, we see a corresponding increase in the f_0 triplets in F_2 and decrease in F_3 (panels (e) and (f)). Although the opposite-spin triplet and singlet correlations cannot reside in the half-metallic regions, in Fig. 7(e), we see the presence of the equal-spin triplet components f_1 and f_2 in the half-metal (F_1). Since these triplet pairs so not suffer from the energetically unfavorable Zeeman splitting, they can subsist in the half-metal. Although f_1 and f_2 propagate throughout the entire F_1 region with a slow spatial variation, these correlations are absent in the other half-metal F_4 which has its magnetization collinear with the adjacent ferromagnet. By rotating the magnetization in F_3 however, Fig. 6(b) shows that $f_{1,2}$ triplet pairs can be created in F_4, peaking when $\theta_3 \approx \pi/6$. This is shown in detail in Fig. 7(f) where the equal-spin triplet pairs have also been amplified in the superconductor.

III. CONCLUSIONS

In summary, motivated by recent theoretical progress and experimental advancements in superconducting spin valves, we have proposed $F_1F_2SF_3$ and $F_1F_2SF_3F_4$ superconducting triplet spin multivalves that host multiple spin valve effects among adjacent F layers. We calculated the superconducting transition temperature, and the spatially-resolved density of states vs the magnetization orientations and layer thicknesses. Our results reveal that due to proximity effects and spin-valve effects involving singlet and triplet conversion and creation, these structures offer stronger superconducting spin-switching and spin-triplet generation compared to the basic *single* SF_1F_2 and F_1SF_2 spin-valve counterparts. In order to provide insight into these switching effects and accurate details of the behavior of the pair correlations in both the singlet and triplet channels, we performed our calculations using a microscopic self-consistent theory that is capable of handling the broad range of length and energy scales involved. This method also allows for multiple Andreev reflections and corresponding resonances in the ballistic regime where the mean free path is much larger than the system thickness. Using this formalism, coupling between layers and quantum effects arising from interfering quasiparticle trajectories within adjacent layers is accounted for. The results shown here demonstrated that the proposed hybrid structures can provide unambiguous signatures of the presence of equal-spin triplet correlations that can arise under relatively weak in-plane external magnetic fields, thus increasing device reliability.

ACKNOWLEDGMENTS

M.A. is supported by Iran's National Elites Foundation (INEF). K.H. is supported in part by ONR and a grant of HPC resources from the DOD HPCMP.

Appendix A: Spin Rotation

Here we outline the spin rotations involving the triplet components (f_0, f_1, f_2), affording a clearer physical interpretation of the results. The central quantity that we use to perform the desired rotations is the spin transformation matrix $\mathcal{T}$ in particle-hole space. The quasiparticle amplitudes transform as,

$$\Psi'_n(x) = \mathcal{T}\Psi_n(x), \tag{A1}$$

where $\Psi_n(x) = (u_{n\uparrow}(x), u_{n\downarrow}(x), v_{n\uparrow}(x), v_{n\downarrow}(x))$, and the prime denotes quantities in the rotated system. The matrix $\mathcal{T}$ can be written solely in terms of the angles that describe the local magnetization orientation. In particular, when the orientation of the exchange fields in a given layer is expressed in terms of the angles given in Eq. (11), we can write:

$$\mathcal{T} = \begin{bmatrix} \cos(\theta_i/2) & -i\sin(\theta_i/2) & 0 & 0 \\ -i\sin(\theta_i/2) & \cos(\theta_i/2) & 0 & 0 \\ 0 & 0 & \cos(\theta_i/2) & -i\sin(\theta_i/2) \\ 0 & 0 & -i\sin(\theta_i/2) & \cos(\theta_i/2) \end{bmatrix}. \tag{A2}$$

Using the spin rotation matrix $\mathcal{T}$, it is also possible to transform the original BdG equations $\mathcal{H}\Psi_n = \epsilon_n\Psi_n$ (Eq. (1)) by performing the unitary transformation: $\mathcal{H}' = \mathcal{T}\mathcal{H}\mathcal{T}^{-1}$, with $\mathcal{T}^\dagger\mathcal{T} = 1$. As is the case under all unitary transformations, the eigenvalues here are preserved, but the eigenvectors are modified in general according to Eq. (A1). Thus we can write,

$$u'_{n\uparrow} = \cos(\theta_i/2)\, u_{n\uparrow} - i\sin(\theta_i/2) u_{n\downarrow}, \tag{A3}$$
$$u'_{n\downarrow} = \cos(\theta_i/2)\, u_{n\downarrow} - i\sin(\theta_i/2) u_{n\uparrow}, \tag{A4}$$
$$v'_{n\uparrow} = \cos(\theta_i/2)\, v_{n\uparrow} - i\sin(\theta_i/2) v_{n\downarrow}, \tag{A5}$$
$$v'_{n\downarrow} = \cos(\theta_i/2)\, v_{n\downarrow} - i\sin(\theta_i/2) v_{n\uparrow}. \tag{A6}$$

Thus for example, the terms involved in calculating the singlet pair correlations (Eq. (3)), obey the following relation between the transformed (primed) and untransformed quantities:

$$u'_{n\uparrow}v'^*_{n\downarrow} + u'_{n\downarrow}v'^*_{n\uparrow} = u_{n\uparrow}v^*_{n\downarrow} + u_{n\downarrow}v^*_{n\uparrow}. \tag{A7}$$

Thus, the terms that dictate the singlet pairing are invariant for any choice of quantization axis, transforming as scalars under spin rotations.

The terms governing the triplet amplitudes on the other hand are not invariant under spin-rotation. The relevant particle-hole products in Eq. (9a) that determine f_0, upon the spin transformations obey the following relationships:

$$\begin{aligned} u'_{n\uparrow}v'^*_{n\downarrow} - u'_{n\downarrow}v'^*_{n\uparrow} &= \cos\theta_i(u_{n\uparrow}v^*_{n\downarrow} - u_{n\downarrow}v^*_{n\uparrow}) \\ &\quad + i\sin\theta_i\left(u_{n\uparrow}v^*_{n\uparrow} - u_{n\downarrow}v^*_{n\downarrow}\right), \\ &= f_0\cos\theta_i + i\sin\theta_i f_2, \end{aligned} \tag{A8}$$

For the equal-spin component f_1, the rotation leaves f'_1 unchanged:

$$u'_{n\uparrow}v'^*_{n\uparrow} + u'_{n\downarrow}v'^*_{n\downarrow} = u_{n\uparrow}v^*_{n\uparrow} + u_{n\downarrow}v^*_{n\downarrow}. \tag{A9}$$

For f'_2 however, it is straightforward to show that

$$\begin{aligned} u'_{n\uparrow}v'^*_{n\uparrow} - u'_{n\downarrow}v'^*_{n\downarrow} &= \cos\theta_i(u_{n\uparrow}v^*_{n\uparrow} - u_{n\downarrow}v^*_{n\downarrow}) \\ &\quad + i\sin\theta_i\left(u_{n\uparrow}v^*_{n\downarrow} - u_{n\downarrow}v^*_{n\uparrow}\right), \\ &= \cos\theta_i f_2 + i\sin\theta_i f_0, \end{aligned} \tag{A10}$$

[1] C. W. J. Beenakker, *Search for Majorana fermions in superconductors*, Ann. Rev. Cond. Matt. **4**, 113 (2013).

[2] C. Nayak, S. H. Simon, A. Stern, M. Freedman, and S. Das Sarma, *Non-Abelian anyons and topological quantum computation*, Rev. Mod. Phys. **80**, 1083 (2008).

[3] M. G. Blamire and J. W. A. Robinson, *The interface between superconductivity and magnetism: understanding and device prospects*, J. Phys.: Cond. Matt. **26**, 453201 (2014).

[4] M. Eschrig, *Spin-polarized supercurrents for spintronics: a review of current progress* Rep. Prog. Phys. **78**, 104501 (2015).

[5] A. Kadigrobov, R. I. Shekhter, and M. Jonson, *Quantum Spin Fluctuations as a Source of Long-Range Proximity Effects in Diffusive Ferromagnet-Superconductor Structures*, Europhys. Lett. **54**, 394 (2001).

[6] A.I. Buzdin, *Proximity effects in superconductor-ferromagnet heterostructures*, Rev. Mod. Phys. **77**, 935 (2005).

[7] F.S. Bergeret, A.F. Volkov, and K.B. Efetov, *Odd triplet superconductivity and related phenomena in superconductor-ferromagnet structures*, Rev. Mod. Phys. **77**, 1321 (2005).

[8] K. Halterman, P.H. Barsic, and O.T. Valls, *Odd Triplet Pairing in Clean Superconductor/Ferromagnet Heterostructures*, Phys. Rev. Lett. **99**, 127002 (2007).

[9] M. Silaev, *Possibility of a long-range proximity effect in a ferromagnetic nanoparticle*, Phys. Rev. B **79**, 184505 (2009).

[10] V.I. Zdravkov, J. Kehrle, G. Obermeier, D. Lenk, H.-A. Krug von Nidda, C. Mller, M. Yu. Kupriyanov, A.S. Sidorenko, S. Horn, R. Tidecks, L.R. Tagirov, *Experimental observation of the triplet spin-valve effect in a superconductor-ferromagnet heterostructure*, Phys. Rev. B **87**, 144507 (2013).

[11] E. Antropov, M. S. Kalenkov, J. Kehrle, V.I. Zdravkov, R. Morari, A. Socrovisciuc, D. Lenk, S. Horn, L.R. Tagirov, A. D. Zaikin, A.S. Sidorenko, H. Hahn, R. Tidecks, *Experimental and theoretical analysis of the upper critical field in ferromagnetsuperconductorferromagnet trilayers*, Supercond. Sci. Technol. **26**, 085003 (2013).

[12] Y.N. Khaydukov, G.A. Ovsyannikov, A.E. Sheyerman, K.Y. Constantinian, L. Mustafa, T. Keller, M.A. Uribe-Laverde, Yu.V. Kislinskii, A.V. Shadrin, A. Kalabukhov, B. Keimer, D. Winkler, *Evidence for spin-triplet superconducting correlations in metal-oxide heterostructures with noncollinear magnetization*, Phys. Rev. B **90**, 035130 (2014).

[13] M.S. Anwar, S.R. Lee, R. Ishiguro, Y. Sugimoto, Y. Tano, S.J. Kang, Y.J. Shin, S. Yonezawa, D. Manske, H. Takayanagi, T.W. Noh and Y. Maeno, *Direct penetration of spin-triplet superconductivity into a ferromagnet in* $Au/SrRuO_3/Sr_2RuO_4$ *junctions*, Nat. Comm. *7*, 13220 (2016).

[14] U. D. Chacn Hernndez, M. B. Fontes, E. Baggio-Saitovitch, M. A. Sousa, and C. Enderlein, *Anti-Lenz supercurrents in superconducting spin valves*, Phys. Rev. B **95**, 184509 (2017).

[15] G. Tkachov, *Magnetoelectric Andreev Effect due to Proximity-Induced Nonunitary Triplet Superconductivity in Helical Metals*, Phys. Rev. Lett. **118**, 016802 (2017).

[16] A. Iovan and V. M. Krasnov, *Signatures of the spin-triplet current in a Josephson spin valve: A micromagnetic analysis*, Phys. Rev. B **96**, 014511 (2017).

[17] J. Cayao and A. M. Black-Schaffer, *Odd-frequency superconducting pairing and subgap density of states at the edge of a two-dimensional topological insulator without magnetism*, Phys. Rev. B **96**, 155426 (2017).

[18] K. Halterman, O. T. Valls, and M. Alidoust, *Spin-controlled superconductivity and tunable triplet correlations in graphene nanostructures* Phys. Rev. Lett. **111**, 046602 (2013).

[19] A. Moor, A.F. Volkov, K.B. Efetov, *Nematic versus ferromagnetic spin filtering of triplet Cooper pairs in superconducting spintronics*, Phys. Rev. B **92**, 180506(R) (2015).

[20] T.S. Khaire, M.A. Khasawneh, W.P. Pratt Jr, N.O. Birge, *Observation of spin-triplet superconductivity in Co-based Josephson junctions*, Phys. Rev. Lett. **104**, 137002 (2010).

[21] S. N. Vdovichev, Yu. N. Nozdrin, E. E. Pestov, P. A. Yunin, A. V. Samokhvalov, *Phase transitions in hybrid SFS structures with thin superconducting layers*, JETP Lett. **104**, 329 (2016).

[22] M. J. Hinton, S. Steers, B. Peters, F. Y. Yang, and T. R. Lemberger, *Evidence for a* π *junction in* $Nb/Ni_{0.96}V_{0.04}/Nb$ *trilayers revealed by superfluid density measurements*, Phys. Rev. B **94**, 014518 (2016).

[23] N. Pompeo, K. Torokhtii, C. Cirillo, A. V. Samokhvalov, E. A. Ilyina, C. Attanasio, A. I. Buzdin, and E. Silva, *Thermodynamic nature of the* 0-π *quantum transition in superconductor/ferromagnet/superconductor trilayers*, Phys. Rev. B **90**, 064510 (2014).

[24] M.G. Flokstra, N. Satchell, J. Kim, G. Burnell, P. J. Curran, S. J. Bending, J. F. K. Cooper, C. J. Kinane, S. Langridge, A. Isidori, N. Pugach, M. Eschrig, H. Luetkens, A. Suter, T. Prokscha, and S. L. Lee, *Remotely induced magnetism in a normal metal using a superconducting spin-valve*, Nat. Phys. **12**, 57 (2016).

[25] S. Kawabata, Y. Asano, Y. Tanaka, and A. A. Golubov, *Robustness of Spin-Triplet Pairing and SingletTriplet Pairing Crossover in Superconductor/Ferromagnet Hybrids*, J. Phys. Soc. Japan **82**, 124702 (2013).

[26] N. G. Pugach, M. Safonchik, T. Champel, M. E. Zhitomirsky, E. Lhderanta, M. Eschrig, C. Lacroix, *Superconducting spin valves controlled by spiral re-orientation in MnSi*, arXiv:1702.08828.

[27] F.S. Bergeret, I.V. Tokatly, *Spin-orbit coupling as a source of long-range triplet proximity effect in superconductor-ferromagnet hybrid structures*, Phys. Rev. B **89**, 134517 (2014).

[28] M. Alidoust and K. Halterman, *Spontaneous edge accumulation of spin currents in finite-size two-dimensional diffusive spinorbit coupled SFS heterostructures*, New J. Phys. **17**, 033001 (2015).

[29] M. Alidoust and K. Halterman, *Long-range spin-triplet correlations and edge spin currents in diffusive spinorbit coupled SNS hybrids with a single spin-active interface*, J. Phys: Cond. Matt. **27**, 235301 (2015).

[30] R.S. Keizer, S.T.B. Goennenwein, T.M. Klapwijk, G. Miao, G. Xiao and A. Gupta, *A spin triplet supercurrent through the half-metallic ferromagnet* CrO_2, Nature **439**, 825 (2006).

[31] V.T. Petrashov, I.A. Sosnin, I. Cox, A. Parsons, C. Troadec, *Giant mutual proximity effects in ferromagnetic/superconducting nanostructures*, Phys. Rev. Lett. **83**, 3281 (1999).

[32] G. Deutscher, F. Meunier, *Coupling between ferromagnetic layers through a superconductor*, Phys. Rev. Lett. **22**, 395 (1969).

[33] S. Oh, D. Youm, and M. R. Beasley, *A superconductive magnetoresistive memory element using controlled exchange interaction*, Appl. Phys. Lett. **71**, 2376 (1997).

[34] Y.V. Fominov, A.A. Golubov, M.Y. Kupriyanov, *Triplet proximity effect in FSF trilayers*, JETP Lett., **77**, 510 (2003).

[35] J. Zhu, I.N. Krivorotov, K. Halterman, O.T. Valls, *Angular dependence of the superconducting transition temperature in ferromagnet-superconductor-ferromagnet trilayers*, Phys. Rev. Lett. **105**, 207002 (2010).

[36] J. Y. Gu, C.-Y. You, J. S. Jiang, J. Pearson, Ya. B. Bazaliy, and S. D. Bader, *Magnetization-Orientation Dependence of the Superconducting Transition Temperature in the Ferromagnet-Superconductor-Ferromagnet System: CuNi/Nb/CuNi*, Phys. Rev. Lett., **89**, 267001 (2002).

[37] L.R. Tagirov, *Low-field superconducting spin switch based on a superconductor/ferromagnet multilayer*, Phys. Rev. Lett., **83**, 2058 (1999).

[38] M. Alidoust, and K. Halterman, *Proximity Induced Vortices and Long-Range Triplet Supercurrents in Ferromagnetic Josephson Junctions and Spin Valves*, J. Appl. Phys. **117**, 123906 (2015).

[39] Ya. V. Fominov, A. A. Golubov, T. Yu. Karminskaya, M. Yu. Kupriyanov, R. G. Deminov, L. R. Tagirov, *Superconducting triplet spin valve*, JETP Letters **91**, 308 (2010).

[40] P. V. Leksin, N. N. Garifyanov, I. A. Garifullin, Ya. V. Fominov, J. Schumann, Y. Krupskaya, V. Kataev, O. G. Schmidt, and B. Bchner, *Evidence for triplet superconductivity in a superconductor-ferromagnet spin valve*, Phys. Rev. Lett. **109**, 057005 (2012).

[41] X. L. Wang, A. Di Bernardo, N. Banerjee, A. Wells, F. S. Bergeret, M. G. Blamire, and J. W. A. Robinson, *Giant triplet proximity effect in superconducting pseudo spin valves with engineered anisotropy*, Phys. Rev. B **89**, 140508(R) (2014).

[42] M. Avdeev, Y. Proshin, *The Solitary Superconductivity in Dirty FFS Trilayer with Arbitrary Interfaces*, J. Low Temp. **185**, 453 (2016).

[43] Y.N. Proshin, Y.A. Izyumov, M.G. Khusainov, *FM/S/FM/S system as the simplest superlattice logical device with two separating recording channels*, Physica C **367**, 181 (2002).

[44] Y.A. Izyumov, Y.N. Proshin, M.G. Khusainov, *Competition between superconductivity and magnetism in ferromagnet/superconductor heterostructures*, Physics-Uspekhi **45**, 109 (2002).

[45] Y. N. Proshin, A. Zimin, N. G. Fazleev, and M. G. Khu-

sainov, *Hierarchy of critical temperatures in four-layered ferromagnet/superconductor nanostructures and control devices*, Phys. Rev. B **73**, 184514 (2006).

[46] M. G. Flokstra, T. C. Cunningham, J. Kim, N. Satchell, G. Burnell, P. J. Curran, S. J. Bending, C. J. Kinane, J. F. K. Cooper, S. Langridge, A. Isidori, N. Pugach, M. Eschrig, and S. L. Lee, *Controlled suppression of superconductivity by the generation of polarized Cooper pairs in spin-valve structures*, Phys. Rev. B **91**, 060501(R) (2015).

[47] Ya. V. Fominov, A. A. Golubov, and M. Yu. Kupriyanov, *superconducting triplet spin valve* JETP Lett. **77**, 510 (2003)

[48] A. Srivastava, L. A. B. Olde Olthof, A. Di Bernardo, S. Komori, M. Amado, C. Palomares-Garcia, M. Alidoust, K. Halterman, M. G. Blamire, J. W. A. Robinsonn, *Magnetization-control and transfer of spin-polarized Cooper pairs into a half-metal manganite*, Phys. Rev. Applied **8**, 044008 (2017).

[49] A. Singh, S. Voltan, K. Lahabi, and J. Aarts, *Colossal Proximity Effect in a Superconducting Triplet Spin Valve Based on the Half-Metallic Ferromagnet* CrO_2, Phys. Rev. X **5**, 021019 (2015).

[50] S. Mironov and A. Buzdin, *Triplet proximity effect in superconducting heterostructures with a half-metallic layer*, Phys. Rev. B **92**, 184506 (2015).

[51] K. Halterman and M. Alidoust, *Half-Metallic Superconducting Triplet Spin Valve*, Phys. Rev. B **94**, 064503 (2016).

[52] Y. Kalcheim, O. Millo, A. Di Bernardo, A. Pal, and J.W.A. Robinson, *Inverse proximity effect at superconductor-ferromagnet interfaces: Evidence for induced triplet pairing in the superconductor*, Phys. Rev. B **92**, 060501(R) (2015).

[53] M. Alidoust, K. Halterman, and O.T. Valls, *Zero-Energy Peak and Triplet Correlations in Nanoscale SFF Spin-Valves*, Phys. Rev. B **92**, 014508 (2015).

[54] M. Alidoust, A. Zyuzin, K. Halterman, *Pure Odd-Frequency Superconductivity at the Cores of Proximity Vortices*, Phys. Rev. B **95**, 045115 (2017).

[55] L. Kuerten, C. Richter, N. Mohanta, T. Kopp, A. Kampf, J. Mannhart, and H. Boschker, *In-gap states in superconducting* $LaAlO_3SrTiO_3$ *interfaces observed by tunneling spectroscopy*, Phys. Rev. B **96**, 014513 (2017).

[56] K. Halterman and O.T. Valls, *Nanoscale ferromagnet-superconductor-ferromagnet switches controlled by magnetization orientation*, Phys. Rev. B **72**, 060514 (2005).

[57] K. Halterman and O.T. Valls, *Proximity effects at ferromagnet-superconductor interfaces*, Phys. Rev. B **65** 014509 (2002).

[58] P. H. Barsic, O. T. Valls, and K. Halterman, *Thermodynamics and phase diagrams of layered superconductor/ferromagnet nanostructures*, Phys. Rev. B **75**, 104502 (2007).

[59] K. Halterman, O.T. Valls and P. H. Barsic, *Induced triplet pairing in clean s-wave superconductor/ferromagnet layered structures*, Phys. Rev. B**77**, 174511 (2008).

[60] K. Halterman and O.T. Valls, *Proximity effects and characteristic lengths in ferromagnet-superconductor structures*, Phys. Rev. B**66**, 224516 (2002)/

[61] K. Halterman and O.T. Valls, *Emergence of Triplet Correlations in Superconductor/Half Metallic Nanojunctions with Spin Active Interfaces*, Phys. Rev. B**80**, 104502 (2009).